International Journal of Nanomedicine

Dovepress
open access to scientific and medical research

Open Access Full Text Article

ORIGINAL RESEARCH

Polydopamine-modified dual-ligand nanoparticles as highly effective and targeted magnetic resonance/photoacoustic dual-modality thrombus imaging agents

This article was published in the following Dove Press journal:
International Journal of Nanomedicine

Yu Zhang[1,2]
Yixin Zhong[1,2]
Man Ye[1]
Jie Xu[1]
Jia Liu[1]
Jun Zhou[1]
Shike Wang[1]
Dajing Guo[1]
Zhigang Wang[2]
Haitao Ran[2]

[1]Department of Radiology, The Second Affiliated Hospital of Chongqing Medical University, Chongqing, People's Republic of China; [2]Chongqing Key Laboratory of Ultrasound Molecular Imaging, Department of Ultrasound, The Second Affiliated Hospital of Chongqing Medical University, Chongqing, People's Republic of China

Background: Platelet activation and subsequent aggregation are the initial stages of thrombosis. A molecular probe that specifically targets activated platelets and remains retained under high shear stress in vivo can enhance the imaging effect to achieve early and accurate diagnosis.
Methods and materials: In this study, we constructed nanoparticles (NPs) using polydopamine to carry two peptides that simultaneously bind integrin αIIbβ3 and P-selectin on activated platelets to enhance the targeting of NPs to thrombus.
Results: The targeting specificity and binding stability of the NPs on red and white thrombi were demonstrated in vitro using a simulated circulatory device and the targeting effect of the NPs on mixed thrombus was studied by magnetic resonance (MR)/photoacoustic (PA) dual-modality imaging in vivo. NPs that were surface modified with both peptides have higher selectivity and retention to red and white thrombi in vitro than NPs with a single or no peptide, and the targeting effect was closely related to the number and distribution of activated platelets as well as the structure and type of thrombus. The NPs also have MR/PA dual-modality imaging functionality, significantly enhancing the imaging of mixed thrombus in vivo.
Conclusion: These dual-targeted NPs have improved targeting specificity and binding stability to different thrombi under high shear stress and are beneficial for the early diagnosis of thrombosis.
Keywords: dual-modality, dual-ligand, targeting effect, thrombus, magnetic resonance imaging, photoacoustic imaging

Introduction

Thrombosis is an important event in vascular disorders and is related to considerable morbidity and mortality.[1,2] Therefore, the early and accurate diagnosis of thrombosis followed by treatment is very important to increase the survival rate of patients and improve the quality of life. Many imaging techniques, such as computed tomography angiography (CTA), ultrasonography and magnetic resonance imaging (MRI), are currently used for identifying and monitoring thrombotic diseases in the clinical setting. However, the early detection and differential diagnosis of thrombi, the distinction between new and old thrombi, and the evaluation of thrombolytic efficacy are still limited.[3] In response to these unmet needs, non-invasive molecular imaging based on targeted nanoparticles (NPs) has attracted wide attention.[4–7]

Although these encouraging studies have demonstrated that NPs modified by specific ligands can be used for the selective delivery of contrast agents to thrombi, the targeting

Correspondence: Haitao Ran
Department of Ultrasound, The Second Affiliated Hospital of Chongqing Medical University, No. 74 Linjiang Road, Yuzhong District, Chongqing 400010, People's Republic of China
Email rht66@163.com

Dajing Guo
Department of Radiology, The Second Affiliated Hospital of Chongqing Medical University, No. 74 Linjiang Road, Yuzhong District, Chongqing 400010, People's Republic of China
Tel +86 236 369 3537
Email guodaj@hospital.cqmu.edu.cn

submit your manuscript | www.dovepress.com
DovePress
http://doi.org/10.2147/IJN.S216603

effect of these NPs in vivo is not as satisfactory as that in vitro, especially in the arteries. Many factors influence the adhesion of the NPs targeting to thrombi, including the ligand affinity, carrier characteristics, target characteristics, target microenvironment, and NPs behavior in circulation.[8] The high shear stress of arterial blood flow is also an important factor. To improve the specificity and stability of the binding of the NPs to thrombi, several methods have been reported: using phase-change materials to prepare NPs to increase the contact area with the thrombi,[9,10] using acoustic radiation force to make the NPs aggregate and slow down near the vascular wall,[11] using specific interactions between ligands and receptors enriched in the target tissues[5,7,12,13] or even using two pairs of ligand-receptor modes[14,15] to increase the adhesion ability of NPs to the targets.

Although NPs with dual ligands[14,15] represent greater adhesion strength than single-ligand NPs in vitro, to our knowledge, there have been no reports on dual-ligand molecular imaging and quantitative analysis of targeted thrombi in vivo of different types and ages, especially in large arterial vessels. Therefore, there is a need to construct a highly efficient dual-ligand molecular probe to target different types of fresh thrombi (ie, white, red and mixed thrombi) and to improve the target effect under the impact of high-speed blood flow in vivo monitored by dual-modality imaging.

One of the most commonly used ligands is RGD/cyclic RGD (cRGD),[5,7,16] a class of short peptides containing arginine-glycine-aspartic acid (Arg-Gly-Asp), for targeting the platelet membrane glycoprotein IIb/IIIa (GPIIb/IIIa, also known as integrin αIIbβ3). However, Merten and his colleagues[17] found that the maximum activation of GPIIb/IIIa occurred in the first 10 s and the GPIIb/IIIa-fibrinogen complex would affect the binding of GPIIb/IIIa with molecular probes carrying the RGD peptide. P-selectin, a member of the selectin family of adhesion molecules, is continuously over-expressed on the membranes of activated platelets in the late stage of thrombosis.[17] Therefore, an increasing number of people have chosen P-selectin as the new target.[9,10,12,13] Selectin-ligand interactions, which mediate leukocyte rolling, can not only activate integrins but also facilitate the binding of integrins to achieve firm adhesion.[14,18] Furthermore Appeldoorn et al[19] demonstrated that GA-EWVDV (a Glu-Trp-Val-Asp-Val pentapeptide modified with gallic acid) was more easily bound to P-selectin and was more specific than other P-selectin ligands.

If NPs can bind to abundant targets expressed on platelet membranes at different stages of thrombosis at any time, their targeting performance may be improved. Based upon this assumption and our previous studies, in order to construct highly effective and targeted photoacoustic (PA)/ magnetic resonance (MR) dual-modality thrombus imaging agents, we prepared core-shell NPs by a double emulsification method with poly-(lactic-co-glycolic acid) (PLGA), paramagnetic iron oxide (Fe_3O_4) NPs and Indian ink, and we adopted a simple surface modification method based on polydopamine (pDA)

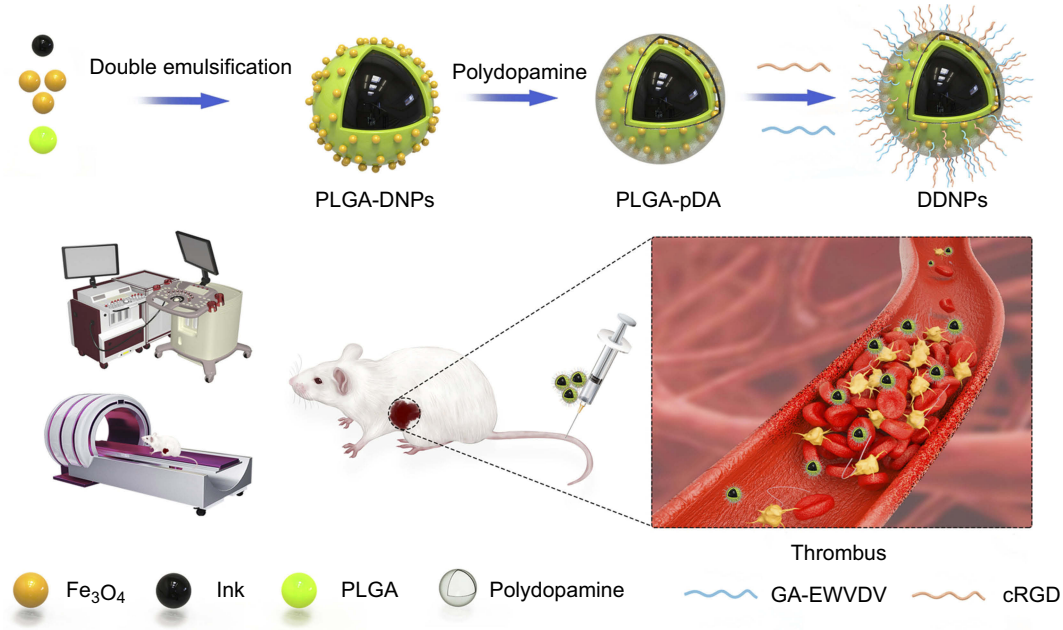

Figure 1 Flow chart of the experimental design.
Abbreviations: PLGA, poly(lactic-co-glycolic acid); DNPs, dual-modality nanoparticles; pDA, polydopamine; DDNPs, dual-modality and dual-ligand nanoparticles; GA-EWVDV, a Glu-Trp-Val-Asp-Val pentapeptide modified with gallic acid; cRGD, cyclic Arg-Gly-Asp.

to simultaneously modify these NPs with cRGD and GA-EWVDV ligands (Figure 1). By studying the general physicochemical properties of the NPs as well as their targeting properties and imaging characteristics to different types of thrombi, we will demonstrate the targeting specificity and binding stability of the NPs on red and white thrombi in vitro and the targeting effect of the NPs on mixed thrombus in vivo. To the best of our knowledge, this is the first time that different types of thrombi were used to study the targeting properties and differences of NPs. This is also the first that dual-ligand-modified NPs have been used for thrombus dual-modality molecular imaging.

Materials and methods

Materials

PLGA (LA:GA =75:25, carboxylic acid end group, molecular weight: 8000, laboratorial reagent, LR) was purchased from Jinan Daigang Biological Material Co., Ltd. (Shangdong, China). Fluorescein isothiocyanate (FITC)-labeled or non-FITC-labeled cRGD peptides, aminomethylcoumarin acetate (AMCA)-labeled or non-AMCA-labeled GA-EWVDV peptides (all peptides were LR) were synthesized by China Peptides Co., Ltd. (Shanghai, China). Iron oxide NPs that had been surface modified with oleic acid (Fe_3O_4, 25 mg/mL, guarantee reagent, GR) were provided by Ocean Nano Technology Co., Ltd. (Springdale, AR, USA). Polyvinyl alcohol (PVA, USP grade), dopamine hydrochloride (analytical reagent, AR) and adenosine 5′-diphosphate sodium salt (ADP, high performance liquid chromatography grade, HPLC Grade) were purchased from Sigma-Aldrich Corporation (St. Louis, MO, USA). India ink (biological reagent, BR) and thrombin (1000 units/0.85 mg solid, BR) were purchased from Solarbio Science & Technology Co., Ltd. (Beijing, China). Collagen-I (4 mg/mL, Chondrex, Inc, cell culture grade) was diluted with 0.02 M HCl at 100 μg/mL. Tris-HCl buffer (10 mM, pH=8.5, LR) was obtained from Beijing Leagene Biotech. Co., Ltd. (Beijing, China). DiI (1,1′-dioctadecyl-3,3,3′3′-tetramethylindocarbocyanine perchlorate, biological stain, BS) was purchased from Beyotime Biotechnology (Jiangsu, China). Agarose (for electrophoresis use) was received from Invitrogen (California, USA). The rest of the reagents were AR.

Preparation and characterization of NPs

A double-emulsion solvent evaporation method was used to prepare PLGA dual-modality NPs (PLGA-DNPs), based on our previous study.[9] One hundred milligrams of PLGA and 80 μL of Fe_3O_4 solution were fully dissolved in 2 mL of dichloromethane as the oil phase. Next, 0.20 mL of India ink (the concentration was diluted to 10% by double-distilled water) and 10 mL of a 4% PVA solution served as the inner and outer aqueous phases, respectively. An ultrasonic liquid processor (Vibra-CellTM VCX-130, Sonics & Materials, Inc., Newtown, CT, USA) was used twice to apply acoustic vibrations for 3 min at 45% power each time to produce a double-emulsion solution. Then, 20 mL of a 2% isopropanol solution was added into the double-emulsion solution and stirred continuously at room temperature for 2 h until the NPs surface solidified and the dichloromethane volatilized. Finally, the PLGA-DNPs were collected by centrifugation and rinsed with double-distilled water.

The polydopamine-coated PLGA-DNPs (PLGA-pDA) were created by incubating PLGA-DNPs in 1 mg/mL dopamine hydrochloride dissolved in a 10 mM Tris buffer (pH 8.5) for 4 h at room temperature with rotation, washed with phosphate buffer saline (PBS) prior and then collected by centrifugation at 10,000 rpm for 5 min.

To make the dual-ligand-modified DNPs (DDNPs), the PLGA-pDA were suspended in PBS buffer with the cRGD and GA-EWVDV peptide mixture (1:1). After 4 h of incubation at room temperature with rotation, the DDNPs were collected by centrifugation. The single-peptide (GA-EWVDV or cRGD)-modified DNPs were prepared by the same method (named EDNPs or RDNPs, respectively).

After an appropriate amount of NPs was suspended in double-distilled water, the morphology and dispersion were observed with an optical microscope (OM, Olympus IX53, Olympus Co. Ltd., Tokyo, Japan), the internal and surface were observed with a transmission electron microscope (TEM, Hitachi 7500, Hitachi Ltd., Tokyo, Japan) and a scanning electron microscope (SEM, Hitachi SU8010, Hitachi Ltd., Tokyo, Japan), respectively. The sizes and zeta potentials of the NPs were determined using a laser particle size analyzer (Zetasizer Nano ZS ZEN 3600, Malvern Instruments Ltd., Worcs, UK). The binding of peptides onto the surface of PLGA-pDA was confirmed by laser scanning confocal microscopy (LSCM, Nikon A1, Nikon Corporation, Tokyo, Japan), and the carrier rate of peptides was determined by flow cytometry (CytoFlex, Beckman Coulter, CA, USA). Atomic absorption spectrometry (TAS-990, Beijing Pgeneral Instruments Co., Ltd., Beijing, China) was used to measure the concentration of iron atoms, and the iron loading rate of the NPs was calculated according to the following formula:

iron loading rate = the actual measured iron mass/the total added iron mass ×100%.

To determine the optimum excitation wavelength and the best imaging concentration of DDNPs in vitro, the PA signals of four concentrations of DDNPs (1.00, 5.00, 10.00, and 20.00 mg/mL) in a 3% agarose gel model were first measured in a PA system (Vevo LAZR, VisualSonics Inc., Toronto, Canada) equipped with a LZ250 (fiber-optic bundles: 25.40×1.25 mm; focal depth: 10 mm; center frequency: 21 MHz; axial resolution: 75 μm) probe. Considering that the number of NPs was linearly related to how much PLGA was used, the concentration of the NPs was indicated by the PLGA quantity in this manuscript. The differences in PA property among the five NPs, PLGA-DNPs, PLGA-pDA, RDNPs, EDNPs, and DDNPs, with the best concentration were examined by irradiating with the optimum laser source of our PA system, while the PA signals were recorded over time. The PA value of the region of interest (ROI) was measured 3 times for each group.

To detect the MR properties of the NPs, 1.00 mg/mL of a dopamine solution, 5.00 mg/mL of the five NPs (PLGA-DNPs, PLGA-pDA, RDNPs, EDNPs, and DDNPs) and 0.25, 0.50, 0.75, 1.00, and 1.25 mg/mL of DDNPs were used. All the NPs were separately added to 2.00 mL Eppendorf tubes and placed in the same plastic container of water to reduce artifacts. MR scanning was performed using a 1.5 T MR scanner (HDXT2012, GE Medical Systems, Fairfield, CT, USA) with a head coil. The parameters of T_2-weighted imaging (T_2WI) were as follows: Fast spin echo (FSE) sequence, repetition time (TR) =1,200.0 ms, echo time (TE) =110.4 ms, flip angle (FA) =90°, field of view (FOV) =20×15 mm, and slice thickness =3.0 mm. The scanning sequences for calculating the transverse relaxation rates (R_2*) of the DDNPs were as follows: TR =52.7 ms, 16 increasing TEs from 1.8 to 28.8 ms, number of excitations =1, and slice thickness =3.0 mm. The data were transferred to an ADW4.6 image workstation (GE Medical Systems, Fairfield, CT, USA), and the Research R_2* software package was used to measure the R_2* values with ROI =20 mm^2.

Targeting specificity and binding stability of NPs in vitro

Preparation of white and red thrombi

The animal experiments were approved by the Animal Ethics Committee of Chongqing Medical University and conducted in accordance with the guidelines of the Institutional Animal Care and Use Committee of Chongqing Medical University. Sprague-Dawley (SD) rats weighing between 200 and 250 g were purchased from the Animal Center of Chongqing Medical University.

White thrombus was prepared by a method similar to that described in a previous publication.[20] Briefly, 5 mL of whole blood was taken from the SD rat's abdominal aorta and drawn into a single-use evacuated tube with EDTA-K2. One mL was taken for platelet counting and the rest for platelet-rich plasma (PRP) preparation. According to Landesberg's method,[21] after the first centrifugation (200 g, 10 min, room temperature), the plasma located immediately above the sediment of red blood cells, including part of the buffy coat (middle layer), was collected and transferred into another anticoagulant tube for the second centrifugation with the same parameter settings. Then, the upper volume of the plasma (platelet-poor plasma, PPP) and the lower half (PRP) were collected into tubes. The concentration of platelets was determined with a Sysmex® XT-2000i 5-diff Automatic Hematology Analyzer (Animal Center of Chongqing Medical University). The PRP, PPP, and whole blood were mixed to form a standardized plasma with a platelet concentration that was approximately 2 times that of whole blood and a hematocrit that was less than or equal to 0.5%. Then, an appropriate amount of thrombin (1000 U/1 mL 0.9% NaCl) was added to the standardized plasma for coagulation to form a white thrombus.

For red thrombus, whole blood was collected in a procoagulant tube until it coagulated at room temperature. Red thrombus can also be prepared by adding thrombin to whole blood to shorten the time of blood coagulation.

Receptor-specific binding studies and blocking studies

To confirm the presence of the activated platelets, white and red thrombi were allowed to adhere to glass slides precoated with a 100 μg/mL collagen-I solution. Then, the adhered platelets were fixed with 4% paraformaldehyde, and their presence on the slides was confirmed by a fluorescently labeled peptide mixture (AMCA-GA-EWVDV and FITC-cRGD), followed by inverted fluorescence microscopy imaging (Olympus IX53, Olympus Co., Ltd., Tokyo, Japan).

Two additional thrombi-adhered slides were used for blocking studies, and the method was as follows: nonfluorescent DDNPs were incubated with the slides for 30 min; then, the slides were washed with PBS and further

incubated with FITC-cRGD and AMCA-GA-EWVDV for 30 min. The rationale was that if the dual-peptide-modified NPs bound their specific target receptors, then the pre-incubation with the DDNPs would possibly occupy many of these receptors and block them from binding the fluorescent peptides in the subsequent step. On the other hand, without pre-incubation of the DDNPs, the fluorescent peptides would successfully stain the respective receptors.

Receptor-specific and stability binding studies in dynamic conditions

Next, eight slides in two groups with red or white thrombi were placed into a simulated circulatory device (Figure 2). After circulation with DiI-labeled DDNPs for 1, 3, 5 and 10 min at a flow rate of 0.40 mL/s, the slides were removed, observed under an inverted fluorescence microscope and imaged with CellSence software to establish the receptor specificity and stability binding studies; PLGA-pDA, RDNPs, and EDNPs were used as control groups. Before each observation, the slides were washed with PBS for 10 s to remove the unstable NPs. The fluorescence intensity of all the slides was measured by ImageJ software.

To observe and confirm the binding and distribution of NPs to thrombi, equal volumes of red or white clots were placed into the same simulated circulation device before circulation with NPs at the same concentration and speed for 30 min. Then, the sections of clots were observed under OM after hematoxylin and eosin (H&E) staining.

Flow cytometry analysis of the binding of NPs to activated platelets in static conditions

The whole blood of the rats was divided into 6 aliquots. First, one of the samples was taken as a control group to determine the gating of platelets with flow cytometer, and the others were incubated with ADP at a concentration of 2×10–5 M for 30 min to activate the platelet population and then fixed with 4% paraformaldehyde for 1 h. The level of activated platelets was assessed by co-staining an aliquot with FITC-cRGD and AMCA-GA-EWVDV and running the sample through the flow cytometer to assess the fluorescence associated with the gated platelet population. Following confirmation of platelet activation, the remaining samples were incubated with the DiI-labeled NPs, PLGA-pDA, RDNPs, EDNPs, and DDNPs at a concentration of 5 mg/mL for 30 min and run through the flow cytometer to analyze the platelet-associated fluorescence. For all analyses, the gated platelet population fluorescence was analyzed at 20,000 counts per sample.

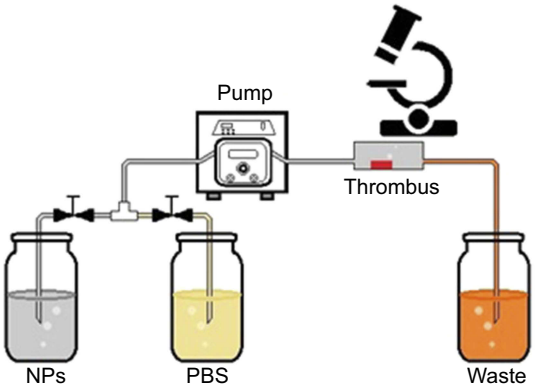

Figure 2 Simulated circulation device in vitro.
Abbreviations: NPs, nanoparticles; PBS, phosphate buffer saline.

Targeting effect and dual-modality imaging performance of NPs in vivo

Preparation of a mixed thrombus

A mixed thrombus was induced by $FeCl_3$ injury to the abdominal aorta of SD rats. Before the experiment, the rats were anaesthetized by injection of pentobarbital sodium (35 mg/kg) and placed in a supine position with the head mounted on the dissecting table. The next process was the same as that previously reported.[22] Briefly, after the abdominal aorta was exposed and passively separated with tweezers, a filter paper approximately 0.8 cm wide soaked in a 10% $FeCl_3$ solution was used to embed the lower segment of the abdominal aorta for 3–5 min, and a parafilm approximately 1.0 cm wide was placed behind the filter paper to prevent the $FeCl_3$ solution from contaminating the surrounding tissues. Then, the filter paper and parafilm were removed, and the abdominal cavity was sutured after washing it with saline.

PA molecular imaging

The PA signals were determined (wavelength ranging from 680 nm to 970 nm) after the abdominal aorta model of wall-adherent thrombosis was successfully achieved to eliminate the interference of the thrombus itself. The rats were then divided into four groups at random (n=3 per group): PLGA-pDA, RDNPs, EDNPs and DDNPs. Then, 1 mL of 5 mg/mL NPs was administered via the tail vein of the rats, and PA molecular imaging was performed after injection for 20 min.

MR molecular imaging

After the abdominal aorta thrombosis model was successfully achieved, twelve rats in four groups (PLGA-pDA, RDNPs,

EDNPs and DDNPs) were scanned by a 3.0 T MR scanner with a rat experiment coil (CG-MUC 18-H300-AP, Shanghai Chenguang Medical Technologies Co., Ltd., Shanghai, China) before and after injection via the tail vein. The T_2WI sequence was performed using the following parameters: turbo spin echo sequence, TR =666.0 ms, TE =62.0 ms, FA =90°, FOV =50.0 mm, and slice thickness =2.0 mm. The areas of the thrombi were measured. The area change rate was calculated according to the following formula: area change rate (%) = (area of the thrombus before injection − area of the thrombus after injection)/(area of the thrombus before injection) ×100%.

Pathological examination of thrombus

After the in vivo imaging was performed, all the rats were sacrificed, and the abdominal aortas of the experimental segment were removed and fixed with 4% paraformaldehyde. After H&E staining, the binding and distribution of NPs to thrombi were observed under a microscope.

Safety evaluation

Three SD rats were used to study the toxicity of DDNPs in vivo. After injection of 1 mL of 5 mg/mL DDNPs via the tail vein, the body weight was recorded every morning, and the overall health of the animals was carefully observed to determine whether there were signs of irritation, pain, discomfort and inflammation. The orbital venous blood was taken from the rats 1 day before injection and 7 days after injection to measure the blood routine and liver and kidney function. The heart, liver, spleen, lung and kidney were taken from the rats 7 days after injection and observed by OM after the H&E staining techniques. Another three rats were injected with 1 mL of saline as a control group.

Data analysis

SPSS 22.0 (Chicago, IL, USA) was used for statistical analysis. All the data are expressed as the mean ± standard deviation. The differences among groups were analyzed by one-way ANOVA, and the difference between the two groups was tested by independent sample and paired *t*-tests. $P<0.05$ indicates that there was a significant difference.

Results and discussion

Characterization of the NPs

Surface modification and functionalization play a key role in controlling the surface properties and conferring new functionalities to materials. However, unless the NPs surface is inherently reactive, decorating the surface with more than one type of functional group by either chemical or physical methods is a time-consuming and complicated process, which is often detrimental to the integrity of the NPs and the production yield. An alternative strategy is to pre-functionalize materials and then produce NPs with these modified materials.[15] But the synthesis needs to be tailored to each functional group, which is equally lengthy and inefficient, and it may alter the properties of the NPs and render them incapable of encapsulating drugs. To overcome these problems, some researchers have used pDA for the surface modification of other nanomaterials.[23–25] Many studies have reported that mussel-inspired dopamine is a novel and effective material with abundant catechol and amino functional groups. These functional groups are helpful to form a super-adherent water-insoluble film (pDA film) on the surface of solid materials and to realize the functionalization of materials.[26,27]

Due to the oxidation and self-polymerization of dopamine under weakly alkaline conditions and the deposition on the surface of materials, DDNPs were successfully constructed in a mixture containing PBS and two peptides at room temperature. The DDNPs appeared black, and they had relatively homogeneous sizes and good dispersion (Figure 3A). TEM revealed that the internal morphology of all the NPs was basically the same; that is, India ink was wrapped in the core, and the lipophilic iron oxide particles were relatively uniformly distributed in the shell. However, compared with the surface of the PLGA-DNPs (Figure 3C and E), the surface of the DDNPs had translucent pDA film deposits (Figure 3B), appeared smooth and had few holes (Figure 3D). LSCM (Figure 3F) showed that most of the red fluorescent DDNPs (DiI-labeled) emitted blue (AMCA-labeled GA-EWVDV peptide) and green (FITC-labeled cRGD peptide) fluorescence, which intuitively demonstrated the successful grafting of dual ligands. At the same time, each fluorescently labeled peptide could show its unique color after being stimulated by a laser, which indirectly indicates that these materials did not interfere with each other. Because these two kinds of fluorescence are not in the same peptide and the pDA method did not involve complex chemical reactions, or pre-activation of functional groups, A flow cytometry scatter plot (Figure 3G) shows that the peptide-grafting rate on DDNPs was up to 99.36%, of which 50.85% was due to NPs with dual ligands at the same time. The average particle size of the DDNPs was 371.27 ±1.12 nm, and the surface potential was −18.87±0.64 mV (Table 1). One-way ANOVA showed that there were

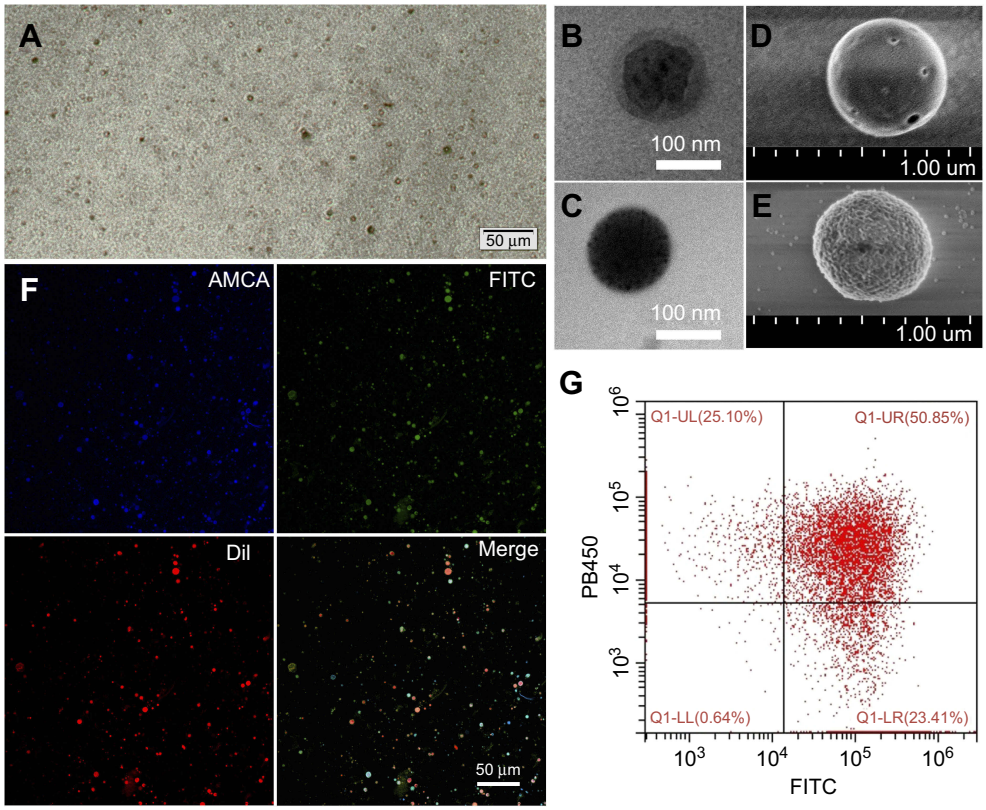

Figure 3 Characteristics of the nanoparticles (NPs).
Notes: (**A**) OM image of DDNPs. (**B**) and (**C**) TEM images of DDNPs and PLGA-DNPs. (**D**) and (**E**) SEM images of DDNPs and PLGA-DNPs. (**F**) LSCM image of DDNPs. (**G**) Flow cytometry scatter plot of DDNPs. NPs with pDA film have a smooth surface and high ligand-grafting rate.
Abbreviations: OM, optical microscope; AMCA, aminomethylcoumarin acetate; FITC, fluorescein isothiocyanate; DiI, 1,1′-dioctadecyl-3,3,3′3′-tetramethylindocarbocyanine perchlorate; DDNPs, dual-modality and dual-ligand nanoparticles.

Table 1 Characteristics of different nanoparticles

Groups	Size (nm)	Zeta potential (mV)	Carrier rate of Fe_3O_4 (%)
PLGA-DNPs	243.57±4.32	−13.33±0.06	/
PLGA-pDA	310.83±4.51	−17.37±0.15	73.40±3.43
RDNPs	331.87±0.45	−17.90±0.40	64.98±0.75
EDNPs	341.07±9.86	−17.37±0.57	65.26±0.54
DDNPs	371.27±1.12	−18.87±0.64	65.11±1.22

Notes: DDNPs not only are larger than PLGA-DNPs and PLGA-pDA but also have a lower zeta potential than do PLGA-DNPs. The carrier rate of Fe_3O_4 of DDNPs was lower than that of PLGA-pDA.
Abbreviations: PLGA, poly(lactic-co-glycolic acid); DNPs, dual-modality nanoparticles; PLGA-pDA, polydopamine-coated PLGA-DNPs; RDNPs, PLGA-pDA modified by the cRGD peptide; EDNPs, PLGA-pDA modified by the GA-EWVDV peptide; DDNPs, dual-modality and dual-ligand nanoparticles.

significant differences among the groups, indicating that the existence of the pDA film and peptides had an impact on the particle size and surface potential of the NPs. Some researchers found that the pDA film thickness was a function of the immersion time and reached a value of up to 50 nm after 24 h.[27] Although large particles have the advantage of carrying high payloads when used as targeted vascular carriers, targeting specificity decreases with enlargement,[28,29] and these large particles are likely to be rapidly recognized and cleared by phagocytes. However, the size of NPs could be easily controlled by tuning the molar ratio or reaction time of dopamine.[23] On the other hand, with the decrease of size, the surface area and energy of the NPs increases and they easily agglomerate. The agglomeration of NPs can cause the embolism of capillaries and even small blood vessels, leading to animal death. If the absolute value of Zeta potential (positive or negative) is higher, the NPs are more stable due to repulsion. In addition, Shao et al[30] have found that NPs with positive surface charges were more toxic than those with negative surface charges and NPs with larger similar charges

were therefore more toxic to the cells. The Zeta potential of the DDNPs is close to −19 mV, and the dispersion is acceptable. However, it is better to use ultrasonic oscillation in a suspension configuration to avoid agglomeration of the NPs as long as possible. The carrier rate of Fe_3O_4 was 65.11±1.22%, which was lower than that of the non-targeting group, but there was no significant difference among the targeting groups. This result may be due to the loss of NPs with the increase in the number of preparation steps. By repeating the preparation process and testing the general properties, we found that the properties of the DDNPs constructed by double emulsification and pDA method were stable and reproducible.

To determine the dual-modality imaging properties of the NPs, we chose India ink and iron oxide NP as the PA and MR contrast agents, respectively. India ink, an optical absorber, has been widely used in the clinic and research because of its good PA imaging and photothermal conversion capability, stable physical and chemical properties, ease of accessibility, inexpensiveness, and nontoxicity.[31–33] Iron oxide NPs, a negative contrast agent for MRI, is also a PA material that can synergize with Indian ink.[9,34,35] Due to the presence of ink and Fe, all five NPs at the best imaging concentration of 5 mg/mL under the optimum excitation wavelength of 790 nm have PA signals in vitro (Figure 4A). In addition, through the PA measurement and one-way ANOVA among groups (Figure 4B), we found that there was no significant difference among the other four groups except for PLGA-DNPs. The results showed that the presence of a pDA film could also enhance the PA signal, but the existence of polypeptides had little effect on the PA signal.

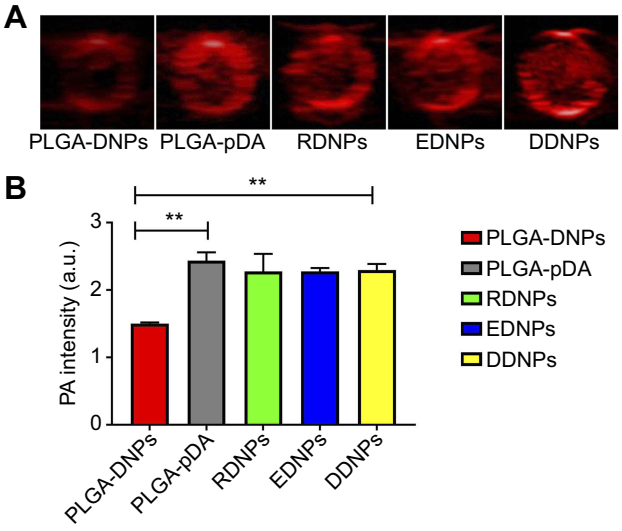

Figure 4 PA properties of the nanoparticles (NPs) in vitro.
Notes: (**A**) PA images of five NPs at the same concentration irradiated by a laser at 790 nm wavelength. (**B**) Quantitative analysis of the PA intensity of the five NPs. (**$P<0.01$) The results confirmed that the presence of the pDA film could enhance the PA signal.
Abbreviations: PA, photoacoustic; PLGA, poly(lactic-co-glycolic acid); DNPs, dual-modality nanoparticles; PLGA-pDA, polydopamine-coated PLGA-DNPs; RDNPs, PLGA-pDA modified by the cRGD peptide; EDNPs, PLGA-pDA modified by the GA-EWVDV peptide; DDNPs, dual-modality and dual-ligand nanoparticles.

All iron-containing NPs exhibited T_2 low signal under the same background on a 1.5 T MR scanner in vitro, except for the dopamine solution, whose signal is close to the water signal (Figure 5A). One-way ANOVA showed that there was no difference in the average signal intensity among the five NPs (Figure 5B). Therefore, we can conclude that the polypeptides and dopamine did not affect the MR signal. The T_2 signal of the DDNPs decreased with increasing concentration, but R_2* increased significantly (Figure 5C and D). This phenomenon is because the iron oxide NPs embedded in the shell are MR negative contrast agents, which will shorten the T_2 time and lead to an increase in R_2*.

Targeting specificity and binding stability of NPs in vitro

In humans, most thrombotic diseases are caused not only by red thrombus but also by white and mixed thrombus. The location, size, composition and age of the thrombus in different patients are also different and complex, which will inevitably affect the choice of treatment methods and the thrombolytic effect. Therefore, taking the types and factors of thrombosis into consideration in the design of the thrombosis model is necessary to make it as close as possible to the human pathophysiological situation. However, in the current models, only red and white thrombosis can be simulated in vitro at present.[20,36] The former is induced in tubes with coagulant promoters, and the latter is mainly prepared by PRP coagulation. Due to the complexity of the formation mechanism, there are no reports on the construction of mixed thrombosis in vitro. Therefore we plan to construct red and white thrombi in vitro to study the targeting specificity and binding stability of DDNPs.

From the images of the receptor-specific binding (Figure 6A and C) and blocking studies (Figure 6B and D) in white and red thrombi and the quantitative data (Figure 6E), we can see that the cRGD and GA-EWVDV peptides can specifically bind to their respective receptors in activated platelets. However, the binding rate decreased significantly in the blocking test, suggesting that the pre-incubation of DDNPs will occupy most of these receptors and prevent their binding to fluorescent peptides. In addition, without pre-incubation, the fluorescence intensity in the white thrombus

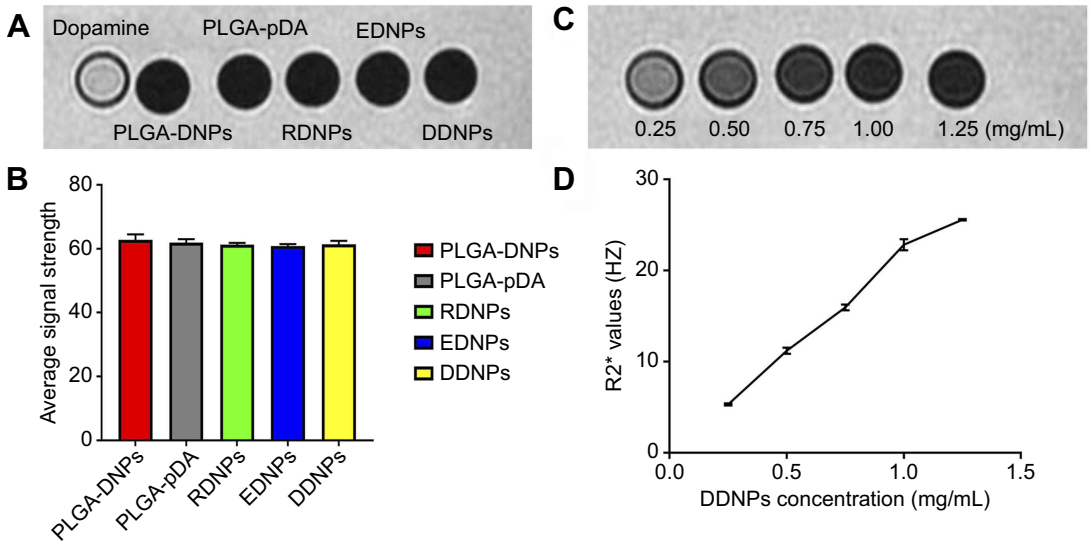

Figure 5 MR properties of the nanoparticles (NPs) in vitro.
Notes: (**A**) and (**C**) T_2-weighted images of dopamine, five NPs at the same concentration, and DDNPs at different concentrations. (**B**) Average signal strength of the five NPs in the same water background. (**D**) Validation curves of the R_2* values of the DDNPs at different concentrations. The results show that iron NPs can shorten the T_2 time of MR and that R_2* increases with concentration.
Abbreviations: R_2*, transverse relaxation rate; PLGA, poly(lactic-co-glycolic acid); DNPs, dual-modality nanoparticles; PLGA-pDA, polydopamine-coated PLGA-DNPs; RDNPs, PLGA-pDA modified by the cRGD peptide; EDNPs, PLGA-pDA modified by the GA-EWVDV peptide; DDNPs, dual-modality and dual-ligand nanoparticles.

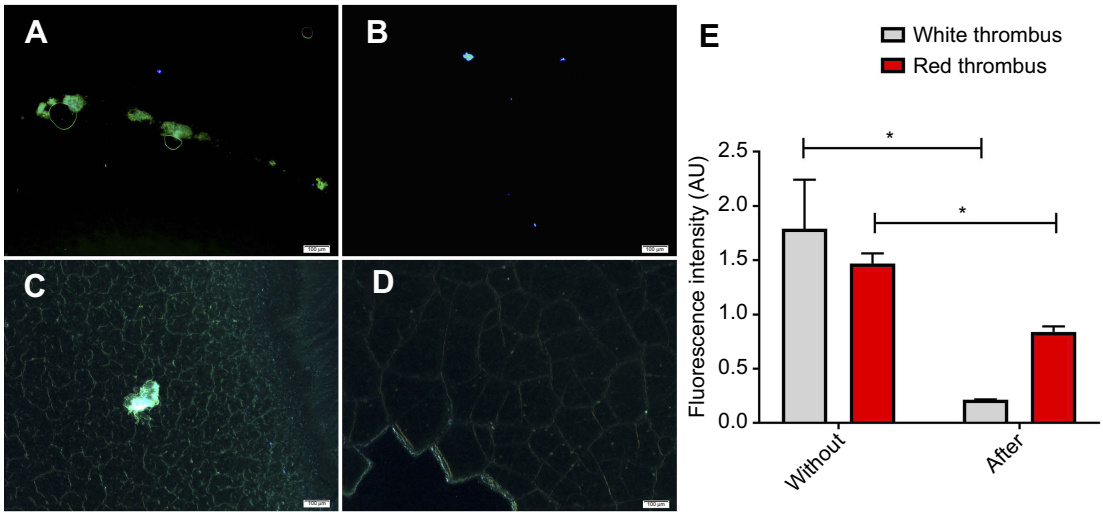

Figure 6 Receptor-specific binding studies and blocking studies observed by inverted fluorescence microscopy after fluorescence staining of GPIIb/IIIa and P-selectin.
Notes: Panels (**A**) and (**B**) respectively show activated platelets in white thrombus without/after pre-incubation with DDNPs. Panels (**C**) and (**D**) show activated platelets in red thrombus without/after pre-incubation with DDNPs. (**E**) Quantitative analysis of the fluorescence intensity. The fluorescence intensity without and after pre-incubation with DDNPs is different, indicating that the nanoparticles can bind to specific targets in the thrombus, especially in the white thrombus. (Scale bar: 100 μm) (*P<0.05).
Abbreviation: DDNPs, dual-modality and dual-ligand nanoparticles.

was higher than that in the red thrombus, indicating that the number of activated platelets in the white thrombus was higher than that in the red thrombus. However, after pre-incubation, the opposite result was found, which confirmed that DDNPs were more likely to bind white thrombus than to bind red thrombus.

The representative fluorescence microscopy images during circulation (Figure 7A and B) and the statistical analysis of the fluorescence intensity after grouping based on the types of thrombi or NPs (Figure 7C) show that the DDNPs can bind to activated platelets in either a red or white thrombus and remain on them in a dynamic flow

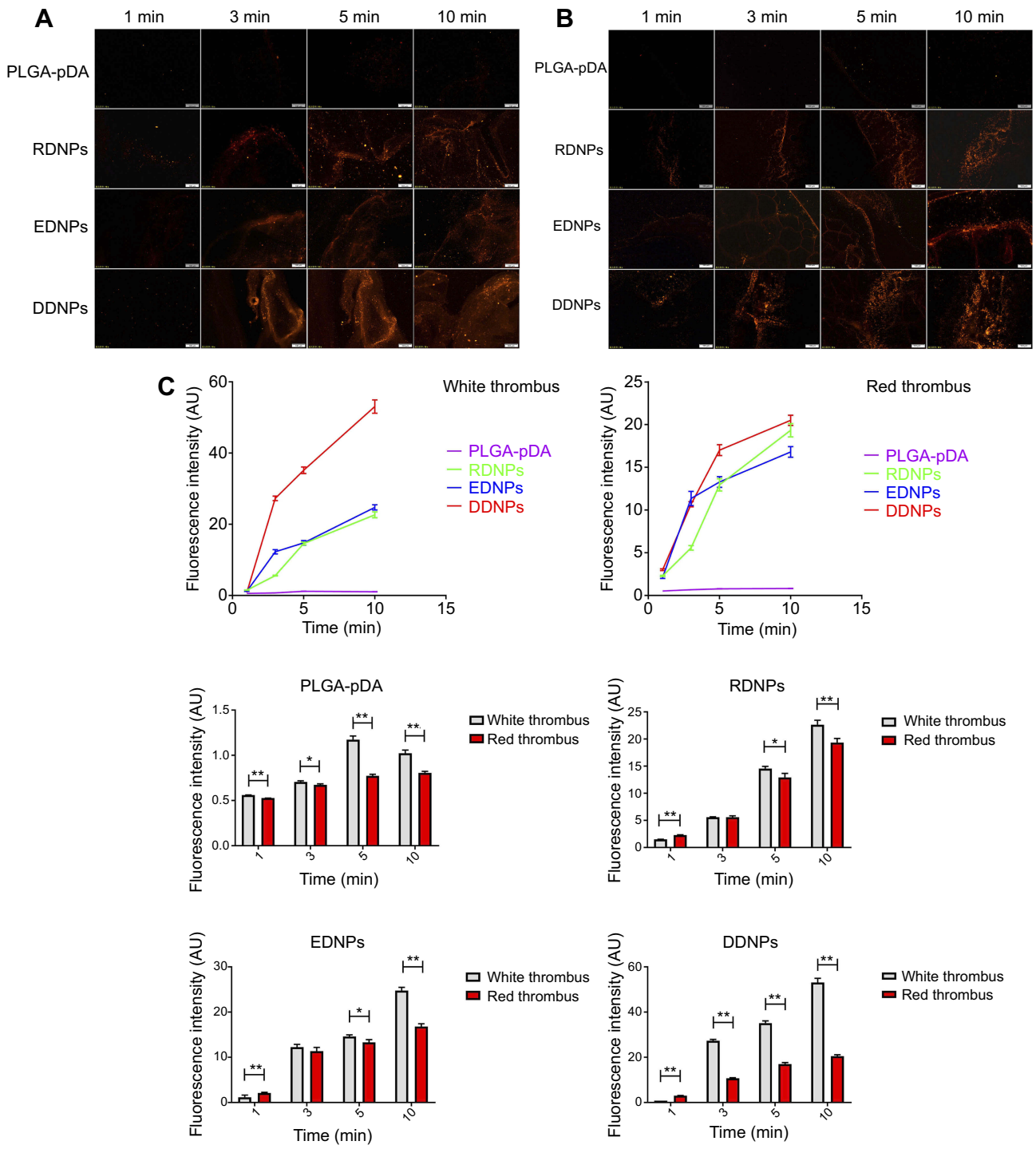

Figure 7 Representative fluorescence microscopy images and quantitative data from the targeting test in a simulated circulation device in vitro.
Notes: (**A**) White thrombus. (**B**) Red thrombus. (**C**) Quantitative analysis of the fluorescence intensity. In a dynamic environment, DDNPs are capable of binding and remain on white/red thrombus at significantly enhanced levels over time compared to non-targeted (PLGA-pDA) and even singly targeted NPs (RDNPs and EDNPs). (Scale bar: 100 μm).
Abbreviations: PLGA-pDA, polydopamine-coated poly(lactic-co-glycolic acid) dual-modality nanoparticles; RDNPs, PLGA-pDA modified by the cRGD peptide; EDNPs, PLGA-pDA modified by the GA-EWVDV peptide; DDNPs, dual-modality and dual-ligand nanoparticles.

environment. Additionally, the DNNP binding level increased significantly over time compared with that of PLGA-pDA or even single-targeted NPs (RDNPs and EDNPs). This phenomenon confirms our theory that the dual ligands will enhance the targeting effect on activated platelets and will be essentially more beneficial to the specific and stable combination of NPs to thrombus under high blood flow shear stress. Furthermore, after

circulation with the same targeted NPs for 5 min, the fluorescence intensity in the white thrombus was significantly higher than that in the red thrombus, also suggesting that the NPs are more likely to bind to white thrombus. However, the difference among the targeting groups in the red thrombus is not as obvious as that in the white thrombus, which may be related to the structure of the thrombus itself. Red thrombus is prone to rupture during a long cycle, resulting in NPs embedded in the gaps, which is difficult to rinse off at the low flow rate.

In dynamic conditions in vitro, according to the results of the pathological sections (Figure 8A and B), white thrombi retract more and have a more compact structure than red thrombi, which may reduce the bulk flow permeability of NPs through the clot. As a result, the NPs (black) are distributed on the surface of the thrombi. This finding is consistent with other researchers' studies, in which cross-linked fibrin and platelet agglomerates impede diffusion into clots for even smaller nanocarriers (<20 nm).[8,37–39] Furthermore, the structure of red thrombi is relatively looser, and the surface will crack after a long time of flushing, which results in passive retention of NPs in the cracks, not just specific binding. Therefore, NPs can be distributed on the surface and inside the thrombi and can aggregate to the area where activated platelets are mainly distributed. However, for both red and white thrombi, the number of NPs in the dual-targeted group was significantly higher than that in the single or non-targeted groups, and the same type of NPs was more likely to target white thrombi. These findings were consistent with our previous fluorescence microscopy images and quantitative analysis results.

Under static conditions in vitro, quantitative analysis of the binding of activated platelets to fluorescent NPs by flow cytometry showed the same results; that is, the binding rate of the dual-targeted group was greater than those of the single-targeted and non-targeted groups, but the difference was not as obvious as that under dynamic conditions (Figure 9). This finding shows that the advantage of dual

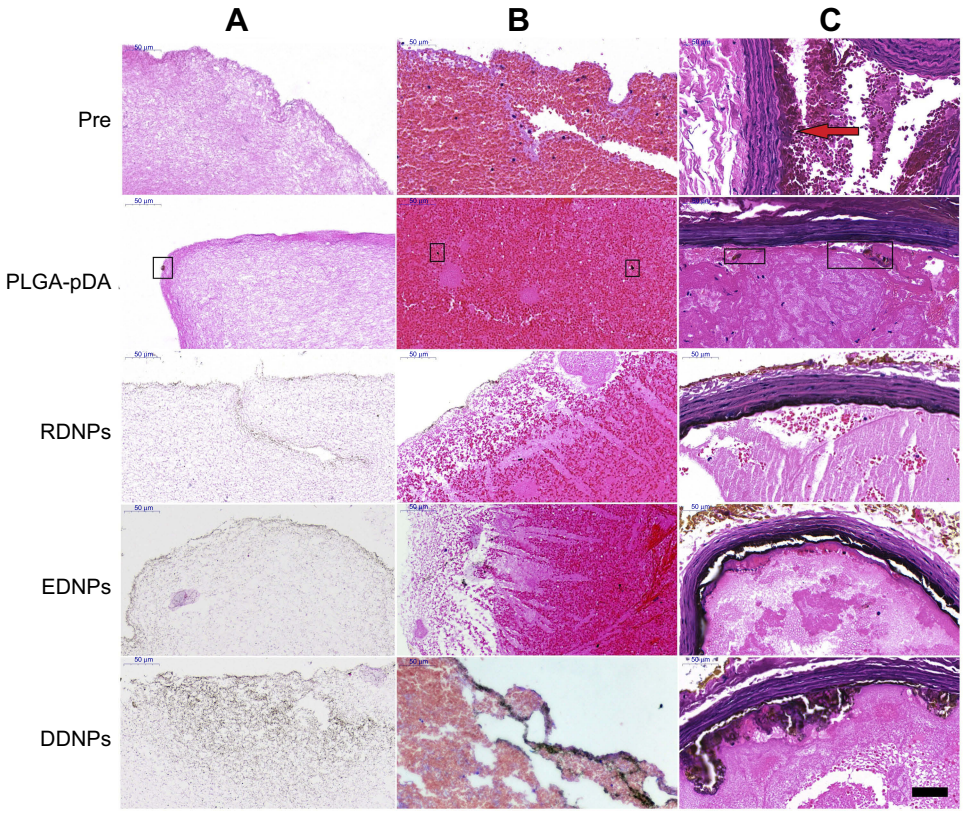

Figure 8 H&E staining images of thrombus sections.
Notes: (**A**) White thrombus. (**B**) Red thrombus. (**C**) Mixed thrombus. Under optical microscope, the continuity of the inner wall of the blood vessel was interrupted (red arrow). In the targeting groups, black NPs were obviously distributed on the surface or inside of the thrombus, especially in the dual-targeted group; in the non-targeted group, only a small number of NPs were distributed (black square). (Scale bar: 50 μm).
Abbreviations: PLGA-pDA, polydopamine-coated poly(lactic-co-glycolic acid) dual-modality nanoparticles; RDNPs, PLGA-pDA modified by the cRGD peptide; EDNPs, PLGA-pDA modified by the GA-EWVDV peptide; DDNPs, dual-modality and dual-ligand nanoparticles.

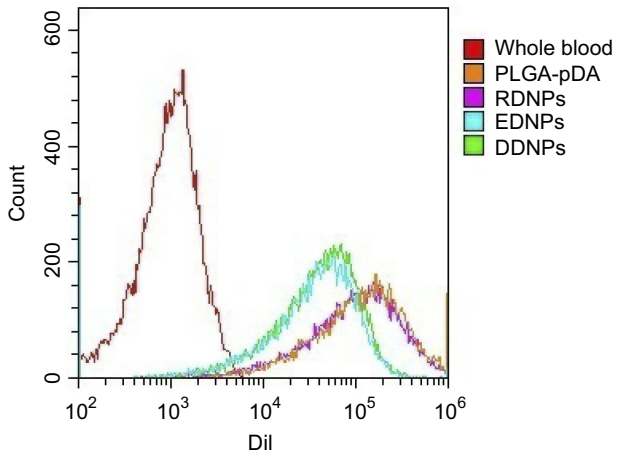

Figure 9 Flow cytometry analysis of the binding of nanoparticles (NPs) to activated platelets under static conditions.

Notes: The binding rate of fluorescently labeled NPs to activated platelets in the targeted groups was higher than that in the non-targeted group, and the binding rate of the dual-targeted group was the highest.

Abbreviations: PLGA-pDA, polydopamine-coated poly(lactic-co-glycolic acid) dual-modality nanoparticles; RDNPs, PLGA-pDA modified by the cRGD peptide; EDNPs, PLGA-pDA modified by the GA-EWVDV peptide; DDNPs, dual-modality and dual-ligand nanoparticles.

ligands is that they can make the combination faster and more stable in dynamic conditions than in static conditions.

Overall, the targeting effect of the DDNPs is better than that of the single or non-targeted groups. In addition, the targeting effect of NPs depends not only on the number and distribution of activated platelets but also on the structure and type of thrombus. Unfortunately, because of the long time and the high flow rate in circulation, the thrombus on the slide will disintegrate or even partly curl and fall off. Therefore, our in vitro experiment did not cycle for a longer time to obtain more information, and we did not study how NPs bind to thrombus under different shear stresses. Another limitation is that we did not use red and white clots at different stages for circulation in vitro. Whether the NPs have targeting differences in different stages of the thrombus remains to be further verified.

Targeting effect and dual-modality imaging performance of NPs in vivo

Thrombosis models in vivo are mainly divided into red thrombosis and mixed thrombosis. The former is induced by slowing down the blood flow resulting in red clots with a large proportion of closely packed erythrocytes,[40] and the latter is formed by mechanical, chemical and other methods of injuring the intima of blood vessels in vivo.[9,22,41,42] Considering that mixed thrombosis is more in line with the human pathophysiological mechanism, we selected mixed thrombosis models in vivo. To prove that DDNPs also have higher targeting specificity and binding stability than do single or non-targeted NPs in vivo and can significantly improve the imaging effect of mixed thrombus under high shear force in vivo, it is necessary to select a suitable imaging modality for visualization research. In addition, the visualization of the delivery and distribution of NPs could play a guiding role in disease therapy.[43–45] However, one of the greatest conundrums of selection is that modalities with the highest sensitivity have relatively poor resolution, while those with high resolution have relatively poor sensitivity.[46] Hence, combining different imaging modalities, such as CT/optical imaging,[47] positron emission tomography (PET)/MRI,[48] and MR/optical imaging,[49–51] to achieve complementary advantages has attracted wide attention. Combining the advantages of optical imaging and ultrasonic imaging, laser-induced PA imaging achieves a great penetration depth and excellent spatial resolution due to the low scattering of acoustics and has developed rapidly as an important molecular imaging technology.[52] In addition to our previous study, many studies have confirmed that a combination of PA and MR in the diagnosis and treatment of diseases can achieve satisfactory results.[9,53–55] Therefore, PA/MR dual-modality imaging combined with pathological observation were used in this study.

The mural thrombus induced by the $FeCl_3$ method was confirmed by pathology to be a mixed thrombus, in which the continuity of the inner wall was interrupted, and a large number of platelet trabeculae were formed. When the abdominal aortic mural thrombus model was established, vascular wall thickening, echo enhancement and lumen stenosis could be observed in all groups under the B-ultrasound mode, and no PA signal was detected in the thrombus itself before injection in the PA mode. The measurement of the PA value (Figure 10B) shows that the PA signal of the thrombus itself is very weak and its influence on the experimental results can be neglected. However, after injection via the tail vein, the non-targeted group had only a small amount of PA signal, while the targeted groups, especially the dual-targeted group, had an obvious amount (Figure 10A). Statistical analysis of the PA signal values (Figure 10B) confirmed that there was a significant difference after injection with dual-targeted NPs compared with non-targeted and single-targeted NPs, which proved that the presence of the dual ligand can significantly enhance the binding rate of NPs to thrombus, leading to the enhancement in the PA signals. There are also differences between the EDNPs and RDNPs, suggesting that the former are more likely to bind stably

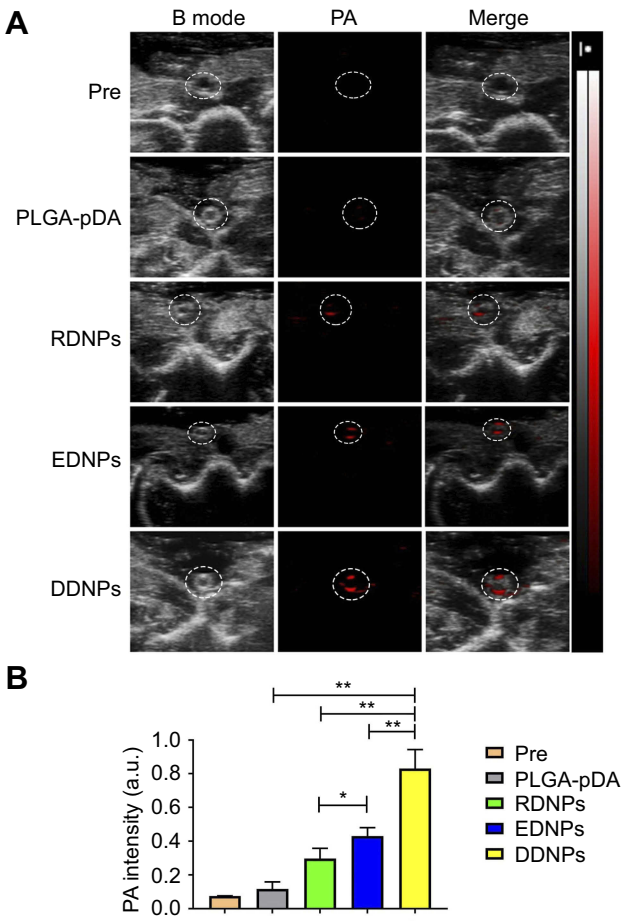

Figure 10 PA molecular imaging.
Notes: (**A**) PAI of mixed thrombus in the abdominal aorta of SD rats before and after intravenous administration of different NPs. (**B**) Quantitative analysis of PA values of the ROI. The PA signals after injection were obvious in the targeted groups, especially in the dual-targeted group. The PA signal of EDNPs is more obvious than that of RDNPs. (*P<0.05, **P<0.01).
Abbreviations: PA, photoacoustic; PAI, photoacoustic imaging; PLGA-pDA, polydopamine-coated poly(lactic-co-glycolic acid) dual-modality nanoparticles; RDNPs, PLGA-pDA modified by the cRGD peptide; EDNPs, PLGA-pDA modified by the GA-EWVDV peptide; DDNPs, dual-modality and dual-ligand nanoparticles.

to thrombus under high shear stress in vivo. This finding is consistent with the literature.[14,18] That is to say, in the middle and late stages of thrombosis, the continuous high expression of P-selectin and the decrease of the platelet rolling speed are more conducive to the combination of NPs and thrombus.

The abdominal aortic mural thrombus of each rat showed high signal intensity on the T_2-weighted sequence, which was in sharp contrast with that of the negative iron-loaded NPs we constructed and provided a theoretical basis for the follow-up work. After injection via the tail vein, the high signal area of the mural thrombus in the non-targeted group (PLGA-pDA) was not significantly decreased compared with that before injection, but the thrombus area in the targeted groups, especially in the dual-targeted group, was significantly decreased (Figure 11A), and the maximum area change rate was 80.00% (RDNPs: 48.48%. EDNPs: 57.50%). The decrease of the high signal area of the thrombus further proves that the thrombus binds to more negative contrast agents, and the binding effect is still DDNP > EDNP > RDNP. Statistical analysis (Figure 11B) confirmed that there were differences in the area measurements before and after injection as well as in the area reduction among groups.

The sections of abdominal aorta and H&E staining after the dual-modality imaging studies also showed the same results. Significant aggregation of black NPs was observed on the thrombus in the targeting groups, especially in the dual-targeted group, while only a small amount of NPs was observed in the black square area of the non-targeted group (Figure 8C).

The results showed that DDNPs could improve the targeting effect both in vivo and in vitro and could significantly enhance the imaging ability of mixed thrombi in vivo, which can provide a strong backing for further targeted thrombolysis research in the future. However, whether there are differences in the targeting of NPs at different time points (representing different stages of thrombosis) and different parts (representing different shear stresses) after injection during PA/MR imaging still requires further study.

Safety evaluation

No death or significant changes in body weight were observed in the SD rats during the 7-day study. The hematology as well as liver and kidney function data showed that the WBC increased slightly 7 days after injection with the DDNPs, while the alamine aminotransferase (ALT) and aspartate aminotransferase (AST) decreased slightly, but there were no significant differences among the other indices (Figure 12A). H&E staining of the heart, liver, spleen, lung and kidney showed no signs of inflammation, necrosis or abnormal cell morphology compared with that of the control group (Figure 12B).

The toxicity test of NPs is an important means to evaluate their clinical safety. However, there is no authoritative reference value for hematological, serum biochemistry and other indicators of experimental animals, and few reagents are specifically used for animal detection. In addition, the differences in animal strain, age, sex and so on make the data between laboratories difficult to compare, so we can only synthesize various indicators to carry

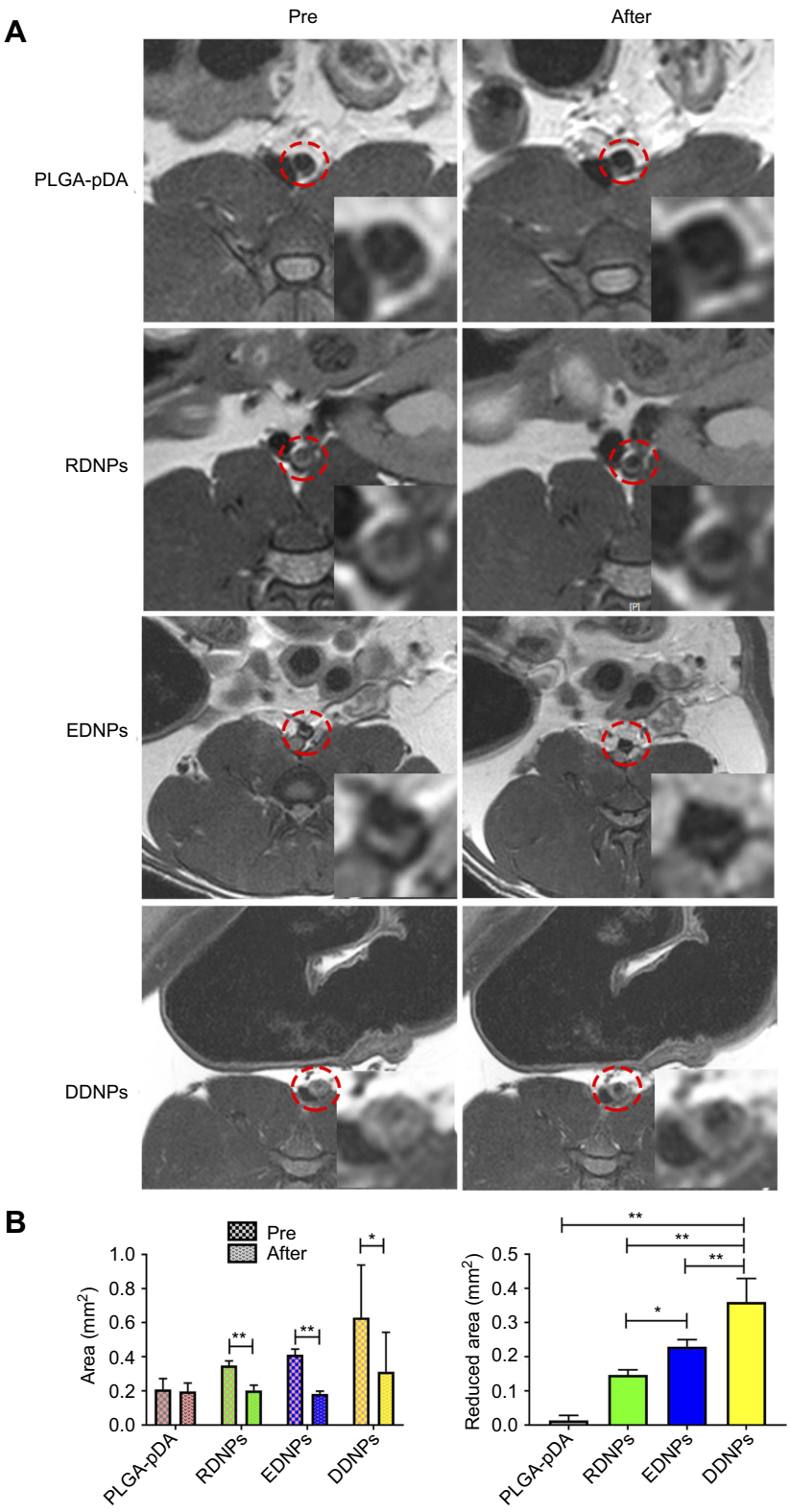

Figure 11 Magnetic resonance molecular imaging.

Notes: (**A**) MRI of mixed thrombus in the abdominal aorta of SD rats before and after intravenous administration of different NPs. Red circles show the abdominal aorta with mixed thrombus. (**B**) Quantitative analysis of the change in the hyperintensity areas of the thrombus. The high signal area of the thrombus was significantly decreased after injection in the targeting groups, especially in the dual-targeted group. (*P<0.05, **P<0.01).

Abbreviations: PLGA-pDA, polydopamine-coated poly(lactic-co-glycolic acid) dual-modality nanoparticles; RDNPs, PLGA-pDA modified by the cRGD peptide; EDNPs, PLGA-pDA modified by the GA-EWVDV peptide; DDNPs, dual-modality and dual-ligand nanoparticles.

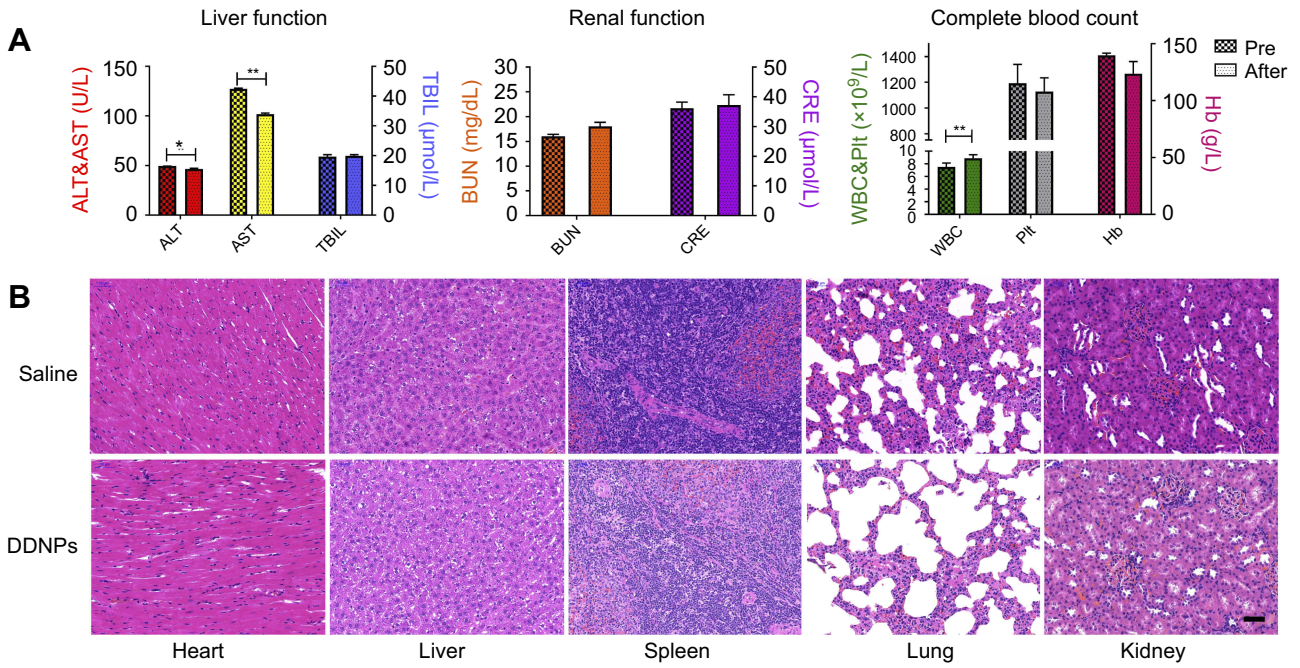

Figure 12 Safety evaluation of DDNPs.
Notes: (**A**) Changes in blood and biochemical indices before and after injection with DDNPs. Although the ALT, AST and WBC were different after injection with DDNPs, the overall condition of the rats was good. (**B**) Pathological H&E staining. No abnormal cell morphologies appeared in the H&E-stained sections of the heart, liver, spleen, lung, or kidney 7 days after injection with DDNPs. (Scale bar: 50 μm) (*P<0.05, **P<0.01).
Abbreviations: ALT, alamine aminotransferase; AST, aspartate aminotransferase; TBIL, total bilirubin; BUN, blood urea nitrogen; CRE, creatinine; WBC, white blood cell; Plt, platelet; Hb, hemoglobin; DDNPs, dual-modality and dual-ligand nanoparticles.

out the toxicity test. We concluded that the constructed DDNPs have certain biological safety.

Conclusion

PA/MR dual-modality NPs with dual ligands were successfully constructed using the double-emulsion method and the pDA method, and the peptide-grafting rate on DDNPs was up to 99.36%, of which 50.85% were dual-peptides. The targeting specificity and binding stability to red and white thrombus in vitro improved, and the targeting effect depended not only on the number and distribution of activated platelets but also on the structure and type of thrombus. The NPs enhanced the targeting effect of mixed thrombus under high shear stress in vivo. Additionally, no matter what type of thrombus, the targeting effect of NPs is DDNP > EDNP > RDNP > PLGA-pDA. However, additional work is needed to evaluate the combination of NPs and thrombus, for instance, whether there are differences in targeting at different time points and under different shear stresses in vitro and in vivo. Further detailed supervision of both fresh and old thrombi at different stages is needed, which will affect the expression of targets in thrombosis.

As highly effective and targeted PA/MR dual-modality thrombus imaging agents, these NPs will help to improve the in vivo targeting ability, especially in arteries. On the other hand, these NPs have the potential ability to encapsulate thrombolytic drugs at the same time, and thus, such efficient targeted NPs can be used as a multi-functional platform to guide thrombolytic therapy under MR/PA dual-modality imaging in the future, and they provide a new method for the integration of diagnosis and treatment.

Acknowledgment

The authors are grateful to the technologists, Weijuan Chen and Shanwei Bai in the Department of Radiology of the Second Affiliated Hospital of Chongqing Medical University for their assistance with MR scanning and American Journal Experts for assistance with language editing. This study was supported by the National Natural Science Foundation of China (grant nos. 81630047 and 81571663).

Disclosure

The authors report no conflicts of interest in this work.

References

1. Absar S, Gupta N, Nahar K, Ahsan F. Engineering of plasminogen activators for targeting to thrombus and heightening thrombolytic efficacy. *J Thromb Haemost*. 2015;13(9):1545–1556. doi:10.1111/jth.13033
2. Siddiqui TI, Kumar KSA, Dikshit DK. Platelets and atherothrombosis: causes, targets and treatments for thrombosis. *Curr Med Chem*. 2013;20(22):2779–2797. doi:10.2174/0929867311320220004
3. Oliveira BL, Caravan P. Peptide-based fibrin-targeting probes for thrombus imaging. *Dalton Trans*. 2017;46(42):14488–14508. doi:10.1039/c7dt02634j
4. Stephens AW, Koglin N, Dinkelborg LM. Commentary to F-GP1, a novel PET tracer designed for high-sensitivity, low-background detection of thrombi: imaging activated platelets in clots-are we getting there. *Mol Imaging*. 2018;17:1–4. doi:10.1177/1536012117749052
5. Zhang Y, Zhou J, Guo D, Ao M, Zheng Y, Wang Z. Preparation and characterization of gadolinium-loaded PLGA particles surface modified with RGDS for the detection of thrombus. *Int J Nanomedicine*. 2013;8:3745–3756. doi:10.2147/IJN.S49835
6. Wang X, Gkanatsas Y, Palasubramaniam J, et al. Thrombus-targeted theranostic microbubbles: a new technology towards concurrent rapid ultrasound diagnosis and bleeding-free fibrinolytic treatment of thrombosis. *Theranostics*. 2016;6(5):726–738. doi:10.7150/thno.14514
7. Cui C, Yang Z, Hu X, et al. Organic semiconducting nanoparticles as efficient photoacoustic agents for lightening early thrombus and monitoring thrombolysis in living mice. *ACS Nano*. 2017;11(3):3298–3310. doi:10.1021/acsnano.7b00594
8. Myerson JW, Anselmo AC, Liu Y, Mitragotri S, Eckmann DM, Muzykantov VR. Non-affinity factors modulating vascular targeting of nano- and microcarriers. *Adv Drug Deliv Rev*. 2016;99:97–112. doi:10.1016/j.addr.2015.10.011
9. Xu J, Zhou J, Zhong Y, et al. Phase transition nanoparticles as multimodality contrast agents for the detection of thrombi and for targeting thrombolysis: in vitro and in vivo experiments. *ACS Appl Mater Interfaces*. 2017;9(49):42525–42535. doi:10.1021/acsami.7b12689
10. Rychak JJ, Lindner JR, Ley K, Klibanov AL. Deformable gas-filled microbubbles targeted to P-selectin. *J Control Release*. 2006;114(3):288–299. doi:10.1016/j.jconrel.2006.06.008
11. Dayton P, Klibanov A, Brandenburger G, Ferrara K. Acoustic radiation force in vivo: a mechanism to assist targeting of microbubbles. *Ultrasound Med Biol*. 1999;25(8):1195–1201. doi:10.1016/s0301-5629(99)00062-9
12. Itoh S, Kawano K, Takeshita K, Maitani Y, Tsuji T. Development of liposomal nanoconstructs targeting P-selectin (CD62P)-expressing cells by using a sulfated derivative of sialic acid. *Pharm Res*. 2014;31(10):2868–2875. doi:10.1007/s11095-014-1383-6
13. Tang R, Chai WM, Yan F, Yang GY, Chen KM. Molecular evaluation of thrombosis using X-ray phase contrast imaging with microbubbles targeted to P-selectin in mice. *Eur Radiol*. 2016;26(9):3253–3261. doi:10.1007/s00330-015-4129-x
14. Eniola AO, Willcox PJ, Hammer DA. Interplay between rolling and firm adhesion elucidated with a cell-free system engineered with two distinct receptor-ligand pairs. *Biophys J*. 2003;85(4):2720–2731. doi:10.1016/S0006-3495(03)74695-5
15. Modery CL, Ravikumar M, Wong TL, Dzuricky MJ, Durongkaveroj N, Sen Gupta A. Heteromultivalent liposomal nanoconstructs for enhanced targeting and shear-stable binding to active platelets for site-selective vascular drug delivery. *Biomaterials*. 2011;32(35):9504–9514. doi:10.1016/j.biomaterials.2011.08.067
16. Srinivasan R, Marchant RE, Gupta AS. In vitro and in vivo platelet targeting by cyclic RGD-modified liposomes. *J Biomed Mater Res A*. 2010;93(3):1004–1015. doi:10.1002/jbm.a.32549
17. Merten M, Thiagarajan P. P-selectin expression on platelets determines size and stability of platelet aggregates. *Circulation*. 2000;102(16):1931–1936. doi:10.1161/01.cir.102.16.1931
18. Ley K. The role of selectins in inflammation and disease. *Trends Mol Med*. 2003;9(6):263–268.
19. Appeldoorn CC, Molenaar TJ, Bonnefoy A, et al. Rational optimization of a short human P-selectin-binding peptide leads to nanomolar affinity antagonists. *J Biol Chem*. 2003;278(12):10201–10207. doi:10.1074/jbc.M209267200
20. Kirchhof K, Welzel T, Zoubaa S, et al. New method of embolus preparation for standardized embolic stroke in rabbits. *Stroke*. 2002;33(9):2329–2333. doi:10.1161/01.str.0000027436.82700.73
21. Landesberg R, Roy M, Glickman RS. Quantification of growth factor levels using a simplified method of platelet-rich plasma gel preparation. *J Oral Maxillofac Surg*. 2000;58(3):297–300. doi:10.1016/s0278-2391(00)90058-2
22. Zhou J, Guo D, Zhang Y, Wu W, Ran H, Wang Z. Construction and evaluation of Fe3O4-based PLGA nanoparticles carrying rtPA used in the detection of thrombosis and in targeted thrombolysis. *ACS Appl Mater Interfaces*. 2014;6(8):5566–5576. doi:10.1021/am406008k
23. Liu Y, Ai K, Liu J, Deng M, He Y, Lu L. Dopamine-melanin colloidal nanospheres: an efficient near-infrared photothermal therapeutic agent for in vivo cancer therapy. *Adv Mater*. 2013;25(9):1353–1359. doi:10.1002/adma.201204683
24. Lin LS, Cong ZX, Cao JB, et al. Multifunctional Fe_3O_4 @ polydopamine core-shell nanocomposites for intracellular mRNA detection and imaging-guided photothermal therapy. *ACS Nano*. 2014;8(4):3876–3883. doi:10.1021/nn500722y
25. Tao W, Zeng X, Wu J, et al. Polydopamine-based surface modification of novel nanoparticle-aptamer bioconjugates for in vivo breast cancer targeting and enhanced therapeutic effects. *Theranostics*. 2016;6(4):470–484. doi:10.7150/thno.14184
26. Gullotti E, Park J, Yeo Y. Polydopamine-based surface modification for the development of peritumorally activatable nanoparticles. *Pharm Res*. 2013;30(8):1956–1967. doi:10.1007/s11095-013-1039-y
27. Lee H, Dellatore SM, Miller WM, Messersmith PB. Mussel-inspired surface chemistry for multifunctional coatings. *Science*. 2007;318(5849):426–430. doi:10.1126/science.1147241
28. Shuvaev VV, Tliba S, Pick J, et al. Modulation of endothelial targeting by size of antibody-antioxidant enzyme conjugates. *J Control Release*. 2011;149(3):236–241. doi:10.1016/j.jconrel.2010.10.026
29. Muro S, Garnacho C, Champion JA, et al. Control of endothelial targeting and intracellular delivery of therapeutic enzymes by modulating the size and shape of ICAM-1-targeted carriers. *Mol Ther*. 2008;16(8):1450–1458. doi:10.1038/mt.2008.127
30. Shao XR, Wei XQ, Song X, et al. Independent effect of polymeric nanoparticle zeta potential/surface charge on their cytotoxicity and affinity to cells. *Cell Prolif*. 2015;48(4):465–474. doi:10.1111/cpr.12192
31. Jian J, Liu C, Gong Y, et al. India ink incorporated multifunctional phase-transition nanodroplets for photoacoustic/ultrasound dual-modality imaging and photoacoustic effect based tumor therapy. *Theranostics*. 2014;4(10):1026–1038. doi:10.7150/thno.9754
32. Magistrelli P, D'Ambra L, Berti S, Feleppa C, Stefanini T, Falco E. Use of India ink during preoperative computed tomography localization of small peripheral undiagnosed pulmonary nodules for thoracoscopic resection. *World J Surg*. 2009;33(7):1421–1424. doi:10.1007/s00268-009-0068-5
33. Williams BB, Khan N, Zaki B, Hartford A, Ernstoff MS, Swartz HM. Clinical electron paramagnetic resonance (EPR) oximetry using India ink. *Adv Exp Med Biol*. 2010;662:149–156. doi:10.1007/978-1-4419-1241-1_21
34. Grootendorst DJ, Jose J, Fratila RM, et al. Evaluation of superparamagnetic iron oxide nanoparticles (Endorem®) as a photoacoustic contrast agent for intra-operative nodal staging. *Contrast Media Mol Imaging*. 2013;8(1):83–91. doi:10.1002/cmmi.1498
35. Feng X, Gao F, Zheng Y. Thermally modulated photoacoustic imaging with super-paramagnetic iron oxide nanoparticles. *Opt Lett*. 2014;39(12):3414–3417. doi:10.1364/OL.39.003414

36. Torno MD, Kaminski MD, Xie Y, et al. Improvement of in vitro thrombolysis employing magnetically-guided microspheres. *Thromb Res*. 2008;121(6):799–811. doi:10.1016/j.thromres.2007.08.017
37. Zaitsev S, Danielyan K, Murciano JC, et al. Human complement receptor type 1-directed loading of tissue plasminogen activator on circulating erythrocytes for prophylactic fibrinolysis. *Blood*. 2006;108(6):1895–1902. doi:10.1182/blood-2005-11-012336
38. Zaitsev S, Zaitzev S, Spitzer D, et al. Targeting of a mutant plasminogen activator to circulating red blood cells for prophylactic fibrinolysis. *J Pharmacol Exp Ther*. 2010;332(3):1022–1031. doi:10.1124/jpet.109.159194
39. Gersh KC, Zaitsev S, Muzykantov V, Cines DB, Weisel JW. The spatial dynamics of fibrin clot dissolution catalyzed by erythrocyte-bound vs. free fibrinolytics. *J Thromb Haemost*. 2010;8(5):1066–1074. doi:10.1111/j.1538-7836.2010.03802.x
40. Hua X, Zhou L, Liu P, et al. In vivo thrombolysis with targeted microbubbles loading tissue plasminogen activator in a rabbit femoral artery thrombus model. *J Thromb Thrombolysis*. 2014;38(1):57–64. doi:10.1007/s11239-014-1071-8
41. Arnljots B, Dahlbäck B. Antithrombotic effects of activated protein C and protein S in a rabbit model of microarterial thrombosis. *Arterioscler Thromb Vasc Biol*. 1995;15(7):937–941. doi:10.1161/01.ATV.15.7.937
42. Chan CC, Ford-Hutchinson A. Potentiation of the inhibitory effect of a thromboxane A2 antagonist (L-640,035) on arterial thrombosis formation in rabbit by the angiotensin converting enzyme inhibitor enalapril. *Eur J Pharmacol*. 1985;110(3):323–328. doi:10.1016/0014-2999(85)90559-x
43. Zhang M, Wang W, Cui Y, et al. Magnetofluorescent Fe_3O_4/carbon quantum dots coated single-walled carbon nanotubes as dual-modal targeted imaging and chemo/photodynamic/photothermal triple-modal therapeutic agents. *Chem Eng J*. 2018;338:526–538. doi:10.1016/j.cej.2018.01.081
44. Wu F, Zhang M, Lu H, et al. Triple stimuli-responsive magnetic hollow porous carbon-based nanodrug delivery system for magnetic resonance imaging-guided synergistic photothermal/chemotherapy of cancer. *ACS Appl Mater Interfaces*. 2018;10(26):21939−21949. doi:10.1021/acsami.8b07213
45. Zhang M, Wu F, Wang W, Shen J, Zhou N, Wu C. Multifunctional nanocomposites for targeted, photothermal, and chemotherapy. *Chem Mater*. 2019;31(6):1847–1859. doi:10.1021/acs.chemmater.8b00934
46. Louie A. Multimodality imaging probes: design and challenges. *Chem Rev*. 2010;110(5):3146–3195. doi:10.1021/cr9003538
47. Kwon SP, Jeon S, Lee SH, et al. Thrombin-activatable fluorescent peptide incorporated gold nanoparticles for dual optical/computed tomography thrombus imaging. *Biomaterials*. 2018;150:125–136. doi:10.1016/j.biomaterials.2017.10.017
48. Ciesienski KL, Yang Y, Ay I, et al. Fibrin-targeted PET probes for the detection of thrombi. *Mol Pharm*. 2013;10(3):1100–1110. doi:10.1021/mp300610s
49. McCarthy JR, Patel P, Botnaru I, Haghayeghi P, Weissleder R, Jaffer FA. Multimodal nanoagents for the detection of intravascular thrombi. *Bioconjug Chem*. 2009;20(6):1251–1255. doi:10.1021/bc9001163
50. Wen AM, Wang Y, Jiang K, et al. Shaping bio-inspired nanotechnologies to target thrombosis for dual optical-magnetic resonance imaging. *J Mater Chem B*. 2015;3(29):6037–6045. doi:10.1039/C5TB00879D
51. Song Y, Huang Z, Xu J, et al. Multimodal SPION-CREKA peptide based agents for molecular imaging of microthrombus in a rat myocardial ischemia-reperfusion model. *Biomaterials*. 2014;35(9):2961–2970. doi:10.1016/j.biomaterials.2013.12.038
52. Gao D, Yuan Z. Photoacoustic-based multimodal nanoprobes: from constructing to biological applications. *Int J Biol Sci*. 2017;13(4):401–412. doi:10.7150/ijbs.18750
53. Zhang L, Sheng D, Wang D, et al. Bioinspired multifunctional melanin-based nanoliposome for photoacoustic/magnetic resonance imaging-guided efficient photothermal ablation of cancer. *Theranostics*. 2018;8(6):1591–1606. doi:10.7150/thno.22430
54. Ye J, Fu G, Yan X, et al. Noninvasive magnetic resonance/photoacoustic imaging for photothermal therapy response monitoring. *Nanoscale*. 2018;10(13):5864–5868. doi:10.1039/C8NR00044A
55. Lu M, Cheng X, Jiang J, et al. Dual-modal photoacoustic and magnetic resonance tracking of tendon stem cells with PLGA/iron oxide microparticles in vitro. *PLoS One*. 2018;13(4):e0193362. doi:10.1371/journal.pone.0193362